On the origin of minimal conductivity at a band crossing

Thibaud Louvet, Pierre Delplace, Andrei A. Fedorenko, and David Carpentier*
Laboratoire de Physique, École Normale Supérieure de Lyon, 46 allée d'Italie, 69007 Lyon, France
(Received 12 May 2015; revised manuscript received 16 July 2015; published 12 October 2015)

Several materials with energy bands crossing giving rise to relativisticlike electronic excitations have recently been discovered beyond the seminal example of graphene. These relativistic phases exhibit remarkable properties, among which is a finite minimal conductivity. While the density of propagating wave states vanishes at the band crossing, the conductivity may remain finite due to evanescent modes in a confined geometry. Studying the generalizations of graphene to three-band models we find that this property is intimately related to the existence of topological Berry phases. We show that the topological robustness of the latter originates from geometrical properties of the underlying lattice, which are encoded into duality properties of the Hamiltonian.

DOI: 10.1103/PhysRevB.92.155116 PACS number(s): 03.65.Vf, 73.43.−f

I. INTRODUCTION

Graphene, discovered in 2004, still remains the canonical example of a semimetal with a band crossing around which excitations are described by a relativistic equation of motion. However, many other realizations have since been identified both in two dimensions [1–4] and in three dimensions [5–17]. Transport measurements provide a powerful tool to probe the properties of relativistic excitations. In graphene, the relativistic nature of the low-energy excitations is at the origin of several characteristic signatures in transport, such as the anomalous quantum Hall effect [18], the Klein tunneling [19], and the nonzero minimal conductivity [19,20]. As opposed to the anomalous quantum Hall effect and the Klein tunneling, the nonzero minimal conductivity is due to evanescent relativistic modes occurring in a confined geometry. While at the band crossing the density of propagating wave states vanishes, transport is still possible through these evanescent modes. Hence, the finite minimal conductivity is a unique signature of the band crossing unveiling the nature of the associated evanescent modes.

To characterize semimetallic phases beyond graphene via transport properties at the band crossing the question of the origin of this minimal conductivity has to be addressed. The minimal conductivity at the band crossing was associated to the Zitterbewegung of Dirac particles, an intrinsic agitation characteristic of ultrarelativistic particles, which leads to diffusive motion even in perfectly clean samples [19,20]. However, whether the presence of Zitterbewegung is sufficient or other constraints are required to infer a finite minimal conductivity is an open question. Among the properties naturally present in graphene at low energy are a chiral symmetry, a pseudospin structure, and a quantized Berry phase acquired by an electron when winding around the crossing point. The latter also gives rise to another two remarkable phenomena: the anomalous quantum Hall effect [21,22] and the topological robustness of graphene [23].

In the present paper, we investigate the origin of the minimal conductivity at the band crossing by considering three-band extensions of graphene. We demonstrate that neither chiral symmetry nor pseudospin structure, nor Zitterbewegung are at the origin of the finite minimal conductivity. On the other hand, at least for the three-band models with chiral symmetry, we relate the nonvanishing minimal conductivity with the existence of topological Berry phases. This relation between the nature of evanescent modes in a confined geometry and a property of propagating wave states of a given gapless relativistic Hamiltonian is reminiscent of the bulk-boundary correspondence in gapped topological phases. To identify the origin of the nonvanishing conductivity we study the simplest models of chiral symmetric semimetals beyond graphene, which are three-band models in two dimensions. These models all possess the same spectrum, chiral symmetry, and exhibit Zitterbewegung. As only some of them exhibit nonvanishing minimal conductivity we can rule out these properties as the origin of this phenomena. Moreover, the conductivity of three-band models corresponding to spin $S = 1$ vanishes ruling out the relevance of the pseudospin structure. Instead, to discriminate between the models with nonvanishing conductivity and those without, we introduce a duality transformation. The duality generalizes the notion of symmetry of Bloch Hamiltonians and allows one to distinguish between models with different nature of evanescent states. We show that the same duality also discriminates between the models with and without topological Berry phase that allows one to link the transport property to the topological one.

The paper is organized as follows. Section II introduces a lattice realization of three-band models with chiral symmetry. We define a duality transformation, which allows us to identify two duality classes in Sec. III. In Sec. IV we discuss the Berry phase properties of a band crossing. We show that the lattice properties at the origin of a topological Berry phase are encoded by none of the standard symmetries of the Hamiltonian but rather by the duality transformation. In Sec. V we study the transport properties of wide junctions using both analytical and numerical Landauer approaches. This allows us to establish a link between a nonvanishing minimal conductivity and a topological Berry phase via duality transformation.

II. CHIRALITY OR SUBLATTICE SYMMETRY

We consider three-band semimetals in two dimensions characterized by two linearly crossing energy bands $n = \pm$ and a third locally flat band $n = 0$, represented in Fig. 1. We focus here on spinless models. This corresponds to

*Corresponding author: David.Carpentier@ens-lyon.fr

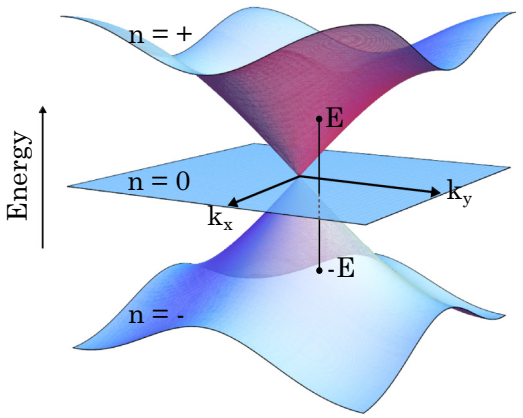

FIG. 1. (Color online) Energy spectrum of a three-band chiral semimetal, which consists of two linear energy bands $n = \pm$ and a flat band $n = 0$ and displays a symmetry $E(\vec{k}) \to -E(\vec{k})$.

the several materials in two and three dimensions [1,2,9]. The energy spectrum $E(\vec{k})$ as a function of the momentum $\vec{k}$ exhibits the symmetry $E(\vec{k}) \to -E(\vec{k})$ at least locally around the crossing point. This spectrum symmetry naturally originates from a chiral symmetry of the corresponding (low-energy) Hamiltonian. This symmetry is represented by a unitary operator C that *anticommutes* with the Hamiltonian: $\mathcal{H} = -C\mathcal{H}C$.

An explicit chiral operator can be defined when considering the pedagogical examples of tight-binding Hamiltonians defined on lattices. Similarly to graphene, only nearest-neighbor couplings can be kept when focusing around the band-crossing points. In this case chiral symmetry corresponds to a sublattice symmetry: couplings are only present between the two sublattices A and B of a bipartite lattice. This is the case of the nearest-neighbor description of graphene on the honeycomb lattice. In the case we consider in this article, three-band crossing implies the existence of three orbitals distributed on three Bravais lattices A_1, A_2 and B of same geometry, as shown on Fig. 2. Chiral symmetry is satisfied if the only couplings t_1, t_2 relevant at low energy are between orbitals on the B and the A_1, A_2 lattices whereas A_1 and A_2 stay uncoupled. The corresponding Bloch Hamiltonian in the orbital basis (A_1, A_2, B) is written

$$H(t_1,t_2;\vec{k}) = \begin{pmatrix} 0 & 0 & t_1 f_1(\vec{k}) \\ 0 & 0 & t_2 f_2(\vec{k}) \\ t_1 f_1^*(\vec{k}) & t_2 f_2^*(\vec{k}) & 0 \end{pmatrix}. \quad (1)$$

Such a Hamiltonian anticommutes with a chirality operator $C = \mathrm{diag}(1,1,-1)$. The complex functions $f_j(\vec{k}) = |f_j(\vec{k})| e^{i\phi_j(\vec{k})}$ encode the geometry of the lattice of couplings. Their amplitudes determine the spectrum of the semimetal: $E_0(\vec{k}) = 0, E_\pm(\vec{k}) = \pm(t_1^2|f_1(\vec{k})|^2 + t_2^2|f_2(\vec{k})|^2)^{\frac{1}{2}}$. A three-band crossing occurs when f_1 and f_2 vanish

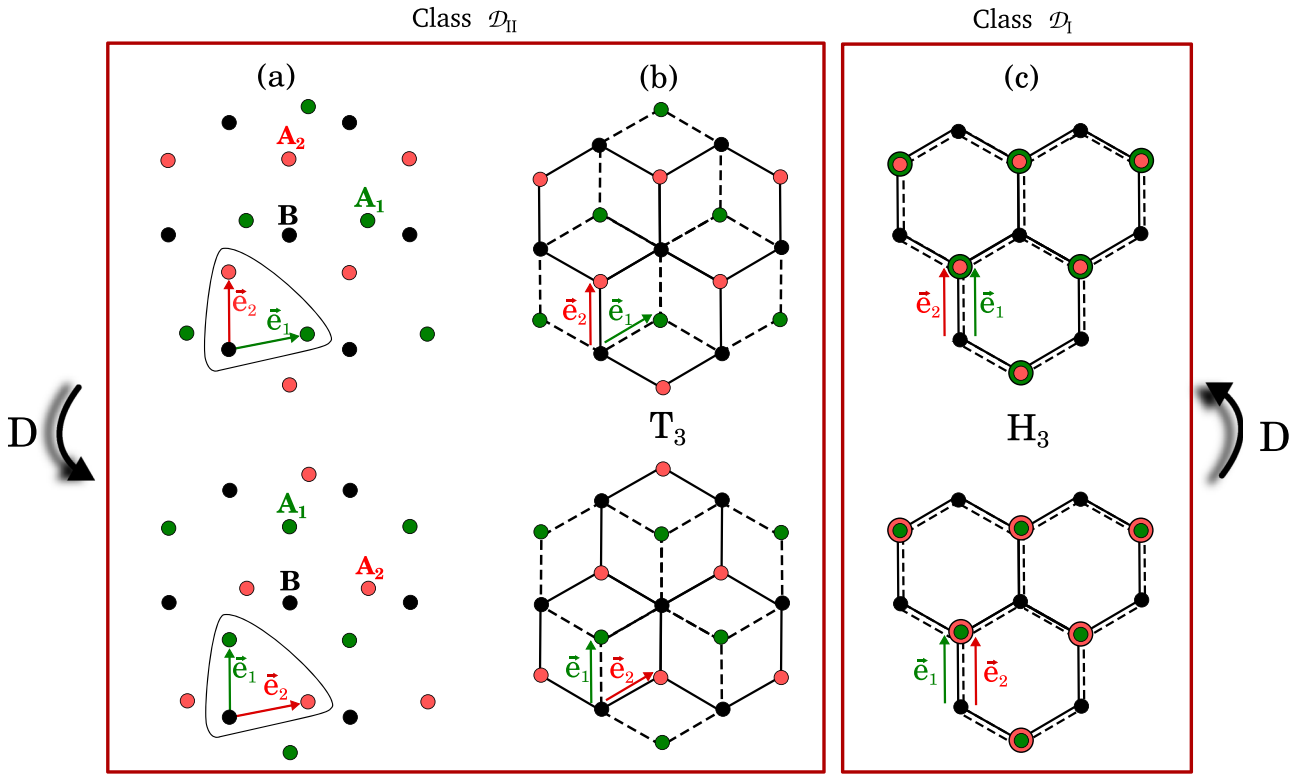

FIG. 2. (Color online) Triangular Bravais lattices with three orbitals (A_1, A_2, and B) per unit cell are represented. The position of the A_1 orbitals is chosen (a) arbitrary, (b) in the center of the BA_1 hexagons for the T_3 lattice, or (c) at the same location than the A_2 orbitals for the H_3 lattice. The duality transformation $\mathcal{D}$ exchanges the location of the orbitals A_1 and A_2 and the hopping amplitudes symbolized by full/dashed lines. The original T_3 lattice is recovered after an inversion in case (b) whereas the dual and the original lattices coincide for the H_3 lattice in case (c).

simultaneously at a point $\vec{K}$ in the Brillouin zone. Generically, additional crystalline symmetries are required to guarantee this vanishing. In the present paper we assume the existence of these band crossings and study some of their transport properties. In particular, we focus on properties, which depend on the phases $\phi_j(\vec{k})$ and which are thus *independent* of the spectrum provided a band crossing occurs.

Quite generally, we will consider chiral symmetric Bloch Hamiltonians describing a three-band semimetal with band crossing at point $\vec{K}$, and whose linear expansion around the crossing takes the form

$$H(\vec{K}+\vec{q}) = \begin{pmatrix} 0 & 0 & \Lambda_{11}q_x+\Lambda_{12}q_y \\ 0 & 0 & \Lambda_{21}q_x+\Lambda_{22}q_y \\ \Lambda_{11}^*q_x+\Lambda_{12}^*q_y & \Lambda_{21}^*q_x+\Lambda_{22}^*q_y & 0 \end{pmatrix}. \quad (2)$$

Such a Hamiltonian is entirely parametrized by a matrix $\Lambda = \{\Lambda_{ij}\}$ of complex coefficients. The phases of the coefficients Λ_{ij} encode the geometry of the underlying lattice. The constraint from the lattice on these phases must be independent of the amplitude of couplings between the orbitals. Hence, it cannot result in a symmetry of the Hamiltonian, which affects energies: we show that it corresponds to a duality in a manner analogous to the Kramers-Wannier duality of statistical mechanics [24].

III. LATTICE GEOMETRY AND DUALITY CONSTRAINTS

The geometry of the lattice can be described by two vectors $\vec{e}_1$ and $\vec{e}_2$ relating a vector of the lattice B to neighbor sites of the A_1 and A_2 lattices, as shown on Fig. 2. The duality transformation $\mathcal{D}$ exchanges the lattices A_1 and A_2, or equivalently the vectors $\vec{e}_1$ and $\vec{e}_2$, while simultaneously exchanging the couplings between B and A_1 orbitals with couplings between B and A_2 orbitals. Quite generally, this duality is an involutive transformation, i.e., $\mathcal{D}^2 = \mathbf{I}$, which relates a Hamiltonian $\mathcal{H}$ on a lattice $\mathcal{L}$ to a Hamiltonian $\tilde{\mathcal{H}}$ on a *different* lattice $\tilde{\mathcal{L}}$. However, on symmetric lattices where initial and dual lattices $\mathcal{L}, \tilde{\mathcal{L}}$ are related by a geometrical transformation $\mathcal{R}$, this duality translates into constraints on Hamiltonians defined on the same lattice (or same Hilbert space). In this case, and focusing for simplicity on nearest-neighbor Hamiltonians, the duality transformation can be recast into the form

$$(DU)H(t_2,t_1;\mathcal{R}\vec{k})(DU)^{-1} = H(t_1,t_2;\vec{k}), \quad (3)$$

where U is a unitary operator, $\mathcal{R}$ is the symmetry relating initial and dual lattices, and D is the operator swapping A_1 and A_2 orbitals:

$$D = \begin{pmatrix} 0 & 1 & 0 \\ 1 & 0 & 0 \\ 0 & 0 & 1 \end{pmatrix}. \quad (4)$$

A very special case, which we call the duality class $\mathcal{D}_{\mathrm{I}}$ corresponds to the situation where two orbitals lie on the same site, i.e., when $\vec{e}_1 = \vec{e}_2 \neq \vec{0}$. In this class, the duality transformation simplifies and U and $\mathcal{R}$ reduce to the identity. In this case, Bloch Hamiltonians encode the geometrical properties of a bipartite lattice, whereas in the other case, which we denote the duality class $\mathcal{D}_{\mathrm{II}}$, the underlying lattices are either Bravais lattices or possess three distinct sublattices. This duality restricts the form of the chiral tight-binding Hamiltonian (1): in the class $\mathcal{D}_{\mathrm{I}}$ we have $f_1(\vec{k}) = f_2(\vec{k})$ while a much weaker constraint $f_1(\vec{k}) = f_2(\mathcal{R}\vec{k})$ holds in class $\mathcal{D}_{\mathrm{II}}$ for symmetric lattices. Specifying this constraint to a local Bloch Hamiltonian (2) around a three-band crossing, the duality in class $\mathcal{D}_{\mathrm{I}}$ implies the condition

$$\frac{\Lambda_{12}}{\Lambda_{11}} = \frac{\Lambda_{22}}{\Lambda_{21}} \equiv \lambda, \quad (5)$$

while generically it only relates Hamiltonians at different crossing points in class $\mathcal{D}_{\mathrm{II}}$. In the following we show that Hamiltonians belonging to the duality class $\mathcal{D}_{\mathrm{I}}$ describe the only three-band semimetals possessing quantized topological Berry windings, which are also those whose conductivity does not vanish at the band crossing and display a pseudodiffusive regime.

To illustrate this relation, let us discuss two nearest-neighbor lattice models of semimetals belonging to both classes. A natural model in class $\mathcal{D}_{\mathrm{I}}$, inspired by graphene, corresponds to a honeycomb lattice with two orbitals on one of the two sublattices, shown in Fig. 2(c). As shown in Appendix A 1, the three bands of this model, which we call H_3, cross at points $\vec{K}$ and $\vec{K}'$ of the Brillouin zone. Around those points, the Bloch Hamiltonian takes the form (2) with a matrix of coefficients

$$\Lambda_{\mathrm{H}_3} = \frac{3a}{2}\begin{pmatrix} t_1 & -\mathrm{i}t_1 \\ t_2 & -\mathrm{i}t_2 \end{pmatrix}, \quad (6)$$

with a being the honeycomb lattice spacing, while the characteristic energy scale of nearest-neighbor couplings is encoded into $t = \sqrt{t_1^2+t_2^2}$. This model satisfies the condition (5) with $\lambda = -\mathrm{i}$ and belongs to the duality class $\mathcal{D}_{\mathrm{I}}$. The T_3 model [25] is again defined on a honeycomb lattice but with additional orbitals A_2 at the center of each hexagon as shown in Fig. 2(b). These orbitals are coupled by an amplitude t_2 only to the B sublattice of the honeycomb lattice, while A_1 and B orbitals on the honeycomb lattices are coupled by t_1 (see Appendix A 2). This model belongs to the duality class $\mathcal{D}_{\mathrm{II}}$, with the inversion $\mathcal{R}\vec{k} = -\vec{k}$ relating initial and dual lattices. Indeed, the Bloch Hamiltonian linearized around the band-touching point $\vec{K}$ is written in the form (2) with

$$\Lambda_{T_3} = \frac{3a}{2}\begin{pmatrix} t_1 & -\mathrm{i}t_1 \\ t_2 & \mathrm{i}t_2 \end{pmatrix}, \quad (7)$$

which does not fulfill the condition (5). Note that when $t_1 = t_2$, this linearized Hamiltonian can be written in the form $H_{\mathbf{K}}(\mathbf{q}) = \hbar v_F \mathbf{S}\cdot\mathbf{q}$, where S_x, S_y and $S_z \equiv \mathrm{diag}(1,-1,0)$ satisfy the spin-1 algebra $[S_i,S_j] = \mathrm{i}\epsilon_{ijk}S_k$. Hence the T_3 model realizes a continuous deformation of spin-1 massless fermions within the duality class $\mathcal{D}_{\mathrm{II}}$.

We now characterize both the topological Berry phase associated with the band crossing, as well as the electronic transport properties around the crossing, which turn out to be associated to the duality class of the semimetal.

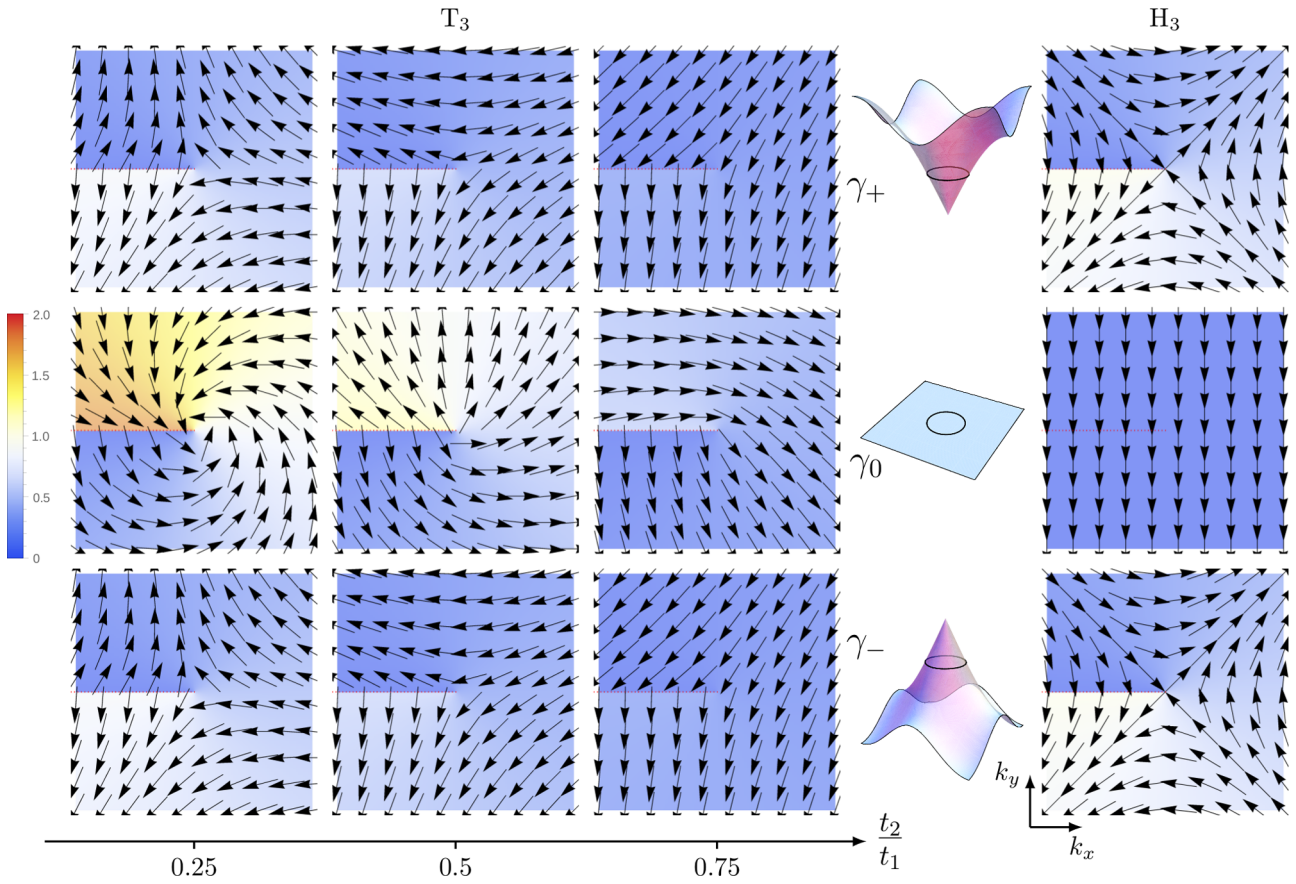

FIG. 3. (Color online) The Berry phase acquired by eigenstates around the band crossing point is shown for the three energy levels $n = -, 0, +$ for nearest neighbors models on the T_3 (left) and on the H_3 model (right). For the H_3 lattice model, the Berry phase γ_n is independent on the coupling amplitudes t_1, t_2 : it is quantized. The windings by $\pm\pi$ in the $\pm$ bands signals the presence of topological Berry vortices at the band crossing points. This is not the case for the T_3 lattice model: the Berry phase continuously depends on the ratio of hopping amplitudes t_2/t_1 for all bands and is not topological.

IV. TOPOLOGICAL BERRY WINDING AROUND A BAND CROSSING

When evolved along a closed loop in momentum space, Bloch eigenstates can acquire a geometrical Berry phase. Moreover, band-touching points act as sources of this Berry phase in two dimensions: it is natural to characterize these points by the Berry phases acquired by the different eigenstates around it. In two dimensions these phases are independent of the choice of loop winding once around the point $\vec{K}$, and are defined as:

$$\gamma_n(\vec{K}) = \frac{-i}{\pi} \oint d\vec{q}.\langle \Psi_n | \vec{\nabla}_{\vec{q}} | \Psi_n \rangle. \tag{8}$$

Besides being only dependent on the homotopy class of the loop around $\vec{K}$, these Berry phases can also be robust against perturbations of the Hamiltonian, which do not lift the band crossing, such as in graphene. In such cases, they are called topological Berry phases. Such a robustness occurs when this Berry winding is quantized. Note that one has to distinguish the topological nature of such a Berry phase from the protection of such a band crossing, which generically involves consideration of crystalline symmetries like in graphene. In the following, we will consider general perturbations of Hamiltonians, which preserve both the chiral symmetry and the band crossing, irrespective of the existence of additional symmetries.

Since the Berry windings are a property of the band crossing solely, they can be conveniently computed from the low-energy Hamiltonian (2). We find that these windings are topological only when the condition (5) is fulfilled: the only semimetals characterized by a topological Berry winding are those of the duality class $\mathcal{D}_{\mathrm{I}}$, with values

$$\gamma_+ = \gamma_- = \mathrm{sgn}\,\mathrm{Im}\,\lambda, \quad \gamma_0 = 0. \tag{9}$$

The calculations are detailed in Appendix A 3: we find that the quantized Berry windings γ_+, γ_- are stable with respect to any perturbation compatible with the duality constraint, i.e., which does not break the geometry of the underlying lattice. Figure 3 shows the phase winding of Bloch eigenstates Ψ_n around the nodal point for the H_3 model of class $\mathcal{D}_I$ and for the T_3 model of class $\mathcal{D}_{II}$. The $\vec{k}$ dependence of the phase is represented by vectors in the two-dimensional momentum space. The color scale gives the accumulated phase with respect to the negative k_x semiaxis. A clockwise vortex corresponds to a winding of π, i.e., to a Berry phase 1. Eigenstates of the H_3 model (6) are characterized by Berry phases $\gamma_\pm = -1$, $\gamma_0 = 0$ as shown in Fig. 3. These Berry phases are in particular robust to variations of hopping amplitudes t_1, t_2. Remarkably for the T_3 model (7),

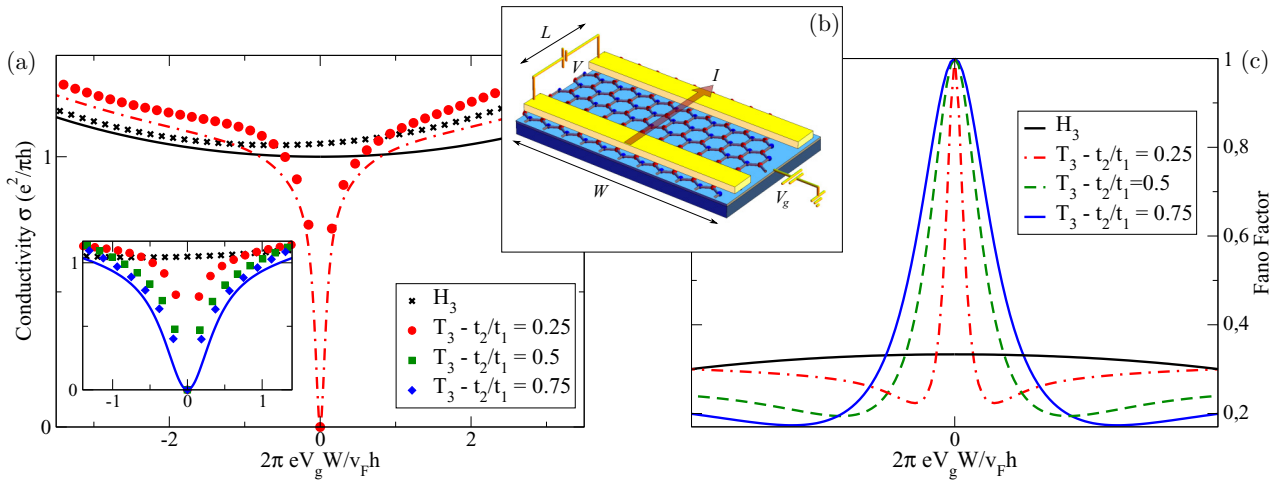

FIG. 4. (Color online) (a) Conductivity and (c) Fano factor as a function of a gate potential V_g applied to the sample in the geometry represented in (b). The inset in (a) shows a zoom on the region of the crossing. Results for nearest-neighbor lattices models on the H_3 and T_3 lattices are shown. They are independent on the coupling amplitudes for the H_3 model, but depend on these couplings for the T_3 model, as illustrated by a choice of three ratio t_2/t_1. The symbols correspond to the results of a numerical Landauer approach on a system of size $L = 20, W = 100$ in units of lattice spacing a. The curves correspond to analytical results of a continuous description around a single cone.

while the Berry phases γ_n are still independent of the path winding, they are shown to vary continuously upon variation of the ratio t_2/t_1 of nearest-neighbor couplings, in agreement with the results of a previous study by Raoux *et al.* [25] (see also Appendix A 3). In particular, they generically take nonquantized values as illustrated by the discontinuity of the vector field.

Thus, for any chiral symmetric semimetal, which does not belong to the $\mathcal{D}_{\rm I}$ class, the Berry phase can take any real value and depends continuously on deformations of the Hamiltonian.

V. MINIMAL CONDUCTIVITY AT THE BAND CROSSING

Transport measurements constitute a powerful tool to probe the physical properties in the vicinity of the Fermi energy. We will show that close to the band crossing electronic transport is related to the phases $\phi_i(\vec{k})$ entering the Hamiltonian in (1) and not to the spectrum. Remarkably, in graphene, when the Fermi level coincides with the twofold band-crossing point, the conductivity of a clean sample was predicted to remain finite despite a vanishing density of states. This result was first derived by considering the conductivity of a narrow strip of graphene between two contact electrodes as shown on Fig. 4.

Let us consider an analogous setup for a three band chiral semimetal, i.e., a finite sample of length L and width W. The conductance of a narrow sample is conveniently calculated from the set of the transmission probabilities T_n of the conduction channel labeled by n through the Landauer formula

$$G = \frac{e^2}{h} \sum_n T_n. \tag{10}$$

The longitudinal conductivity σ is related to this conductance as $\sigma = LW^{-1}G$. The explicit calculation of the transmission probabilities T_n requires solving the Schrödinger equation piecewise and matching the solutions at the boundaries of the sample. Confinement of the sample between the leads gives rise to zero-energy evanescent states. At the band crossing, the conductivity depends entirely on the nature of these evanescent states. Prior to an explicit calculation of the conductivity, it is instructive to consider the current operator $j_x(\vec{k}) = \langle \partial_{k_x} H(\vec{k}) \rangle_\psi$ defined from the tight-binding Bloch Hamiltonian (1). Introducing the amplitudes $(\psi_{A_1}, \psi_{A_2}, \psi_B)$ of the electronic wave function in the three sublattices the longitudinal current can be expressed as $j_x(\vec{k}) = 2\mathrm{Re}\,\{\psi_B(\vec{k})[\partial_{k_x} f_i(\vec{k})\psi^*_{A_i}(\vec{k})]\}$ and is found to be proportional to the amplitude ψ_B on the B sublattice [26]. This hints that electronic transport at the band crossing will occur provided the zero-energy evanescent modes have a nonvanishing component on the B sublattice.

As expected from the previous qualitative argument, the existence of a finite minimal conductivity at the threefold band crossing point is uniquely determined by the nonvanishing weight of the wave function on the hub lattice B as we have checked using a Landauer description of transport in Appendix B 1. From (2), this component is found to satisfy

$$\Lambda . \begin{pmatrix} q_x \\ q_y \end{pmatrix} \psi_B = 0. \tag{11}$$

Hence a necessary condition for the existence of a nonvanishing minimal conductivity at the band crossing is simply $\det \Lambda = 0$. This constraint is equivalent to the duality constraint (5) defining the class $\mathcal{D}_{\rm I}$: the only three-band semimetals with a nonvanishing minimal conductivity belong to this duality class $\mathcal{D}_{\rm I}$. Reciprocally, any model in this duality class has a finite minimal conductivity, as shown in Appendix B 1b. Moreover for the H_3 lattice model, this minimal conductivity corresponds exactly to the value $\sigma^{(\min)} = e^2/(\pi h)$ predicted for graphene. This result remains valid for any model in the dual class $\mathcal{D}_{\rm I}$, or more generally $\det \overline{\sigma} = [e^2/(\pi h)]^2$ for an anisotropic dispersion relation. In contrast, any three-band chiral symmetric semimetal in class $\mathcal{D}_{\rm II}$ possesses a vanishing conductivity $\sigma^{(\min)} = 0$ in every direction. Beyond the minimal conductivity, the fluctuations of this conductivity

can also be considered : their amplitude is encoded in the ratio between the shot-noise power and the averaged current, the so-called Fano factor. This Fano factor is related to the transmission coefficients as $F = \sum_n T_n(1-T_n)/\sum_n T_n$. We find that this factor F takes a constant value $F = 1/3$ within the duality class $\mathcal{D}_{\rm I}$, a value already encountered in graphene [20] and characteristic of diffusive metals [27]. Such a result demonstrates that for all semimetals in this class the transport through narrow, perfectly clean junctions displays the characteristic features of diffusive metals.

We have evaluated the conductivity of different lattice models in the geometry of Fig. 4. We compare the analytical results to a numerical Landauer approach to check for possible inter-crossing-point effects, neglected in the analytical approach. Numerical calculations were performed using the KWANT code [28], based on a Green's function recursive technique to evaluate the transmission amplitude across a sample. Typical samples of dimensions $L = 20$, $W = 100$ in lattice units were considered, with semi-infinite one-dimensional (1D) chains modeling the leads. A good agreement is found between both approaches. The results for the H_3 model are shown as a function of the Fermi energy, or gate potential V_g, in Fig. 4: the conductivity exhibits a plateau around the band crossing point $V_g = 0$, corresponding to $\sigma = e^2/(\pi h)$. The results of a similar study for the T_3 model are also shown in Fig. 4 and display a collapse of the conductivity around the band crossing point $V_g = 0$ for three different values of the couplings between orbitals (inset). Figure 4 displays the analytical results for the dependance of the Fano factor on the gate potential V_g. We show that for the T_3 model $F(V_g = 0) = 1$, whereas for the H_3 model the Fano factor reaches the value $F = \frac{1}{3}$ at the band crossing, characteristic of a disordered metal as expected for class $\mathcal{D}_{\rm I}$. Finally, let us mention that for graphene the result of the Landauer formula for a narrow junction can be recovered for a long junction by an approach based on the Kubo formula [29]. While this equivalence remains valid for three-band semimetals in the dual class $\mathcal{D}_{\rm I}$, it does not hold beyond it: we found that the Kubo conductivity for the T_3 model diverges at the band crossing (see Appendix B 2), as opposed to the vanishing Landauer conductivity for a narrow junction, in agreement with a previous result in the disordered limit [30].

VI. CONCLUSION

As follows from the results of this paper, the occurrence of a transport regime at the band crossing with a nonvanishing conductivity through evanescent modes is not a generic property of linear dispersion relations near this crossing nor a hallmark of relativistic physics of the associated electronic excitations such as the Zitterbewegung, chiral symmetry or pseudospin structure.

However, at least for three-band models with chiral symmetry in two dimensions, a nonvanishing conductivity is surprisingly found to be related to a quantized Berry phase of the Bloch bands. This result highlights a new connection between the nature of evanescent states (and associated minimal conductivity) and a topological property (topological Berry phase) of wavelike eigenstates. This evanescent-bulk state correspondence is reminiscent of the standard bulk-edge correspondence in topological insulating phases. Here, the nonvanishing conductivity through evanescent states and the quantized Berry phase of Bloch states both follow from lattice properties encoded into a duality property (class $\mathcal{D}_{\rm I}$), in contrast with a symmetry property. Generically, the special lattice properties required to belong the duality class $\mathcal{D}_{\rm I}$ are not met. In that case the Berry phase is then found to be not quantized and the conductivity vanishes at the band crossing. This puts in perspective the existence of a minimal conductivity in graphene that turns out to fulfill a very special criteria.

Our results open a new route to a fine probe of band crossings through evanescent states that discriminates different fundamental transport properties (conductivity and noise) of semimetals. They constitute a key step toward the understanding of the properties of evanescent modes in semimetals. Along these lines, we have extended our analysis to a band crossing described by the simple Hamiltonian $H(\vec{q}) = S_x q_x + S_y q_y$, with S_x, S_y satisfying a spin-S algebra [31]. Again, we find that the Berry topological winding and the minimal conductivity are correlated and vanish for integer spin S. Beyond this, several directions are particularly promising for future investigations, such as to release the constraint of chiral symmetry or extensions to three-dimensional semimetals [32,33].

ACKNOWLEDGMENTS

We thank F. Piéchon for stimulating discussions about the T_3 model, as well as A. Akhmerov and X. Waintal for helpful advice with the KWANT package. This work was supported by the grants ANR Blanc-2010 IsoTop and ANR Blanc-2012 SemiTopo from the french Agence Nationale de la Recherche.

APPENDIX A: BAND PROPERTIES

1. H_3: Three-band hexagonal model

The three-band hexagonal model is a possible generalization of graphene, adding an extra orbital exactly on one sublattice as shown on Fig. 2. To write the Bloch Hamiltonian of our system, consider the triangular Bravais lattice with three sites per unit cell. The spectrum therefore consists of three energy bands, each carrying one third of the electronic states. The Hamiltonian for a given value of $\varphi = \arctan(\frac{t_2}{t_1})$ reads, in the (A_1, A_2, B) basis:

$$H(\vec{k}) = \begin{pmatrix} 0 & 0 & f(\vec{k})\cos\varphi \\ 0 & 0 & f(\vec{k})\sin\varphi \\ f^*(\vec{k})\cos\varphi & f^*(\vec{k})\sin\varphi & 0 \end{pmatrix}, \quad \text{(A1)}$$

where $f(\vec{k}) = t(1 + e^{i\vec{k}.\vec{u}_1} + e^{i\vec{k}.\vec{u}_2})$. $\vec{u}_1 = \frac{\sqrt{3}a}{2}(-\vec{e}_x + \sqrt{3}\vec{e}_y)$, and $\vec{u}_2 = \frac{\sqrt{3}a}{2}(\vec{e}_x + \sqrt{3}\vec{e}_y)$ are basis vectors of the triangular Bravais lattice. Note that, due to the duality constraint corresponding to class $\mathcal{D}_I$, matrix elements H_{A_1B} and H_{A_2B} have equal complex phase. The spectrum does not depend on φ. It consists of a flat band at zero energy $\varepsilon_0(\vec{k}) = 0$ and two dispersive bands $\varepsilon_\pm(\vec{k}) = \pm|f(\vec{k})|$.

In sublattice basis, the eigenstates of (A1) have the form:

$$\Psi^{\pm}(\vec{k}) = \frac{1}{\sqrt{2}}\begin{pmatrix}\cos\varphi e^{-i\theta}\\ \sin\varphi e^{-i\theta}\\ \pm 1\end{pmatrix}, \quad \varepsilon(\vec{k}) = \pm|f(\vec{k})|; \quad \text{(A2a)}$$

$$\Psi^{0}(\vec{k}) = \begin{pmatrix}-\sin\varphi\\ \cos\varphi\\ 0\end{pmatrix}, \quad \varepsilon(\vec{k}) = 0, \quad \text{(A2b)}$$

where $\theta = \arg[f(\vec{k})]$.

The three bands touch at the corners of the first Brillouin zone $\vec{K} = \frac{4\pi}{3\sqrt{3}a}\vec{u}_x$ and $\vec{K}' = -\vec{K}$. In the vicinity of band-touching point $\vec{K}$, the low-energy Hamiltonian reads:

$$H(\vec{K}+\vec{q}) = \hbar v_F \begin{pmatrix}0 & 0 & q_-\cos\varphi\\ 0 & 0 & q_-\sin\varphi\\ q_+\cos\varphi & q_+\sin\varphi & 0\end{pmatrix}. \quad \text{(A3)}$$

where we denote $q_\pm = q_x \pm iq_y$, and with $v_F = 3at/2\hbar$, a the honeycomb lattice spacing and t the characteristic hopping strength. When $\varphi = 0$ or $\pi/2$ ($t_1 = 0$ or $t_2 = 0$), the 2D Dirac Hamiltonian of graphene is recovered, with an extra flat band acting as a mere spectator.

2. T_3 model

The T_3 lattice consists of a honeycomb lattice with one additional site at the center of each hexagon, connected to one of the sublattices of the honeycomb lattice (see Fig. 2): it can be seen as two shifted honeycomb lattices sharing one sublattice. The dual lattices A_1B and A_2B are related by inversion symmetry $\mathcal{R}\vec{k} = -\vec{k}$; hence, this model belongs to duality class $\mathcal{D}_{II}$. The 3×3 Bloch Hamiltonian at wave vector $\vec{k}$ reads:

$$H(\vec{k}) = \begin{pmatrix}0 & 0 & f(\vec{k})\cos\varphi\\ 0 & 0 & f^*(\vec{k})\sin\varphi\\ f^*(\vec{k})\cos\varphi & f(\vec{k})\sin\varphi & 0\end{pmatrix}, \quad \text{(A4)}$$

where the function $f(\vec{k})$ has been defined in the previous section. The spectrum is given by: $\varepsilon(\vec{k}) = 0, \pm|f(\vec{k})|$. It is identical to the spectrum of the H_3 model.

Let us have a look at the eigenstates of Hamiltonian (A4). Corresponding wave functions read:

$$\Psi^{\pm}(\vec{k}) = \frac{1}{\sqrt{2}}\begin{pmatrix}\cos\varphi e^{-i\theta}\\ \sin\varphi e^{i\theta}\\ \pm 1\end{pmatrix}, \quad \varepsilon(\vec{k}) = \pm|f(\vec{k})|; \quad \text{(A5a)}$$

$$\Psi^{0}(\vec{k}) = \begin{pmatrix}-\sin\varphi e^{i\theta}\\ \cos\varphi e^{-i\theta}\\ 0\end{pmatrix}, \quad \varepsilon(\vec{k}) = 0, \quad \text{(A5b)}$$

where $\theta = \arg[f(\vec{k})]$.

The low-energy Hamiltonian expanded around band-touching point $\vec{K}$ reads:

$$H(\vec{K}+\vec{q}) = \hbar v_F \begin{pmatrix}0 & 0 & q_-\cos\varphi\\ 0 & 0 & q_+\sin\varphi\\ q_+\cos\varphi & q_-\sin\varphi & 0\end{pmatrix}, \quad \text{(A6)}$$

3. Berry phase around the nodal point

Upon winding around the band-touching point, electrons in the nth energy band pick up a so-called Berry phase γ_n:

$$\gamma_n(\vec{K}) = \frac{-i}{\pi}\oint d\vec{q}.\langle\Psi_n|\vec{\nabla}_{\vec{q}}|\Psi_n\rangle, \quad \text{(A7)}$$

where Ψ_n is the corresponding Bloch eigenstate. The integrand in (A7) is the Berry connection

$$\vec{A}_n(\vec{q}) = -i\langle\Psi_n|\vec{\nabla}_{\vec{q}}|\Psi_n\rangle = \mathrm{Im}(\langle\Psi_n|\vec{\nabla}_{\vec{q}}|\Psi_n\rangle). \quad \text{(A8)}$$

Here we compute the Berry connection and the Berry phase (A7) for eigenstates of the general Hamiltonian of the $\mathcal{D}_I$ duality class, and for the T_3 model of the $\mathcal{D}_{II}$ duality class.

a. $\mathcal{D}_I$ class

The general low-energy $\mathcal{D}_I$ class Hamiltonian can be written in the following form:

$$H(\vec{q}) = \begin{pmatrix}0 & 0 & \alpha(q_x+\lambda q_y)\\ 0 & 0 & \beta(q_x+\lambda q_y)\\ \alpha^*(q_x+\lambda^* q_y) & \beta^*(q_x+\lambda^* q_y) & 0\end{pmatrix}. \quad \text{(A9)}$$

The spectrum is given by: $\varepsilon_\pm(\vec{q}) = \pm\sqrt{|\alpha|^2+|\beta|^2}|q_x+\lambda q_y|, \varepsilon_0(\vec{q}) = 0$. We may fix the total energy scale without loss of generality by setting $|\alpha|^2+|\beta|^2 = 1$. The eigenstates of (A9) read:

$$\Psi_\pm(\vec{q}) = \frac{1}{\sqrt{2}}\begin{pmatrix}\alpha\frac{q_x+\lambda q_y}{|q_x+\lambda q_y|}\\ \beta\frac{q_x+\lambda q_y}{|q_x+\lambda q_y|}\\ \pm 1\end{pmatrix}, \quad \varepsilon_\pm = \pm|q_x+\lambda q_y|, \quad \text{(A10a)}$$

$$\Psi_0(\vec{q}) = \begin{pmatrix}-\beta^*\\ \alpha^*\\ 0\end{pmatrix}, \quad \varepsilon_0 = 0. \quad \text{(A10b)}$$

We then compute the Berry connection (A8) for the lower and upper dispersive bands Ψ_+ and Ψ_- (A10a):

$$A_x^\pm = \mathrm{Im}(\langle\Psi_\pm|\partial_{q_x}|\Psi_\pm\rangle) = -\frac{q_y}{2|q_x+\lambda q_y|^2}\mathrm{Im}(\lambda) \quad \text{(A11a)}$$

$$A_y^\pm = \frac{q_x}{2|q_x+\lambda q_y|^2}\mathrm{Im}(\lambda). \quad \text{(A11b)}$$

Integrating along a loop of constant $||\vec{q}||$ yields the Berry phase:

$$\begin{aligned}\gamma_\pm &= \frac{1}{\pi}\int_0^{2\pi} q d\theta A_\theta^\pm = \int_0^{2\pi} q d\theta \left(\frac{q_x}{q}A_y^\pm - \frac{q_y}{q}A_x^\pm\right)\\ &= \left(\frac{1}{2\pi}\int_0^{2\pi}\frac{d\theta}{|\cos\theta + \lambda\sin\theta|^2}\right)\mathrm{Im}(\lambda)\\ &= \mathrm{sgn}[\mathrm{Im}(\lambda)]. \end{aligned} \tag{A12}$$

The Berry phase is quantized and in particular does not change under continuous variations of the Hamiltonian parameters, provided the duality constraint of class $\mathcal{D}_I$ is preserved. For the flat band, (A10b) immediately gives $\vec{A} = \vec{0}$, and thus $\gamma_0 = 0$.

The H_3 model belongs to the $\mathcal{D}_I$ class; it corresponds to the case $\lambda = -\mathrm{i}$. Thus from (A12) the invariants associated with eigenstates of the H_3 model are $\gamma_\pm = -1$, $\gamma_0 = 0$. Alternatively, one can recover these results by an explicit calculation from the eigenstates (A2).

b. T_3 model: An example from the $\mathcal{D}_{11}$ class

We now consider low-energy excitations of the T_3 model. Using expression (A5a) for the eigenstates of the dispersive bands with $f(\vec{K}+\vec{q}) \simeq q_x - \mathrm{i}q_y = qe^{-\mathrm{i}\theta}$, the Berry connection is given by:

$$\vec{A}_\pm = -\tfrac{1}{2}\cos 2\varphi \vec{\nabla}_{\vec{q}}\theta, \tag{A13}$$

which yields for the Berry phase (A7):

$$\gamma_\pm = -\cos 2\varphi. \tag{A14}$$

Similarly, eigenstates of the flat band (A5b) are characterized by a Berry phase:

$$\gamma_0 = 2\cos 2\varphi. \tag{A15}$$

These phases vary continuously with the hopping parameter φ, and vanish when $\varphi = \pi/4$. The only source of Berry phases is the band-crossing point itself: this manifests into the robustness of their value beyond the linear approximation. Keeping the general expression $f(\vec{k}) = |f(\vec{k})|e^{\mathrm{i}\phi(\vec{k})}$ and integrating along an isoenergy contour $|f(\vec{k})| = \text{const.}$ as in Ref. [25] still yields the windings (A14) and (A15).

c. Three-band chiral linear crossing with topological Berry phase

Here we show that for a three-band crossing described by the linearized Hamiltonian (2) to have a topological Berry phase, it must belong to the duality class $\mathcal{D}_I$. In particular, it thus has a finite minimal conductivity. First, consider the Λ_{ij} coefficients characterizing Hamiltonian (2). Through a global change of energy scale and phase of the Hamiltonian, they are cast under the form:

$$\Lambda = \begin{pmatrix}\cos\varphi e^{ib} & \cos\varphi e^{ib}\nu\\ \sin\varphi & \sin\varphi\mu\end{pmatrix}, \tag{A16}$$

where φ is defined by $\tan\varphi = \frac{|\Lambda_{21}|}{|\Lambda_{11}|}$. In the context of lattice models it corresponds to the ratio of hoppings, as in (A1) and (A4). Eigenstates from the dispersive bands now read:

$$\psi_\pm = \frac{1}{\sqrt{2}}\begin{pmatrix}\cos\varphi e^{ib}\frac{k_x+\nu k_y}{\varepsilon_{\vec{k}}}\\ \sin\varphi\frac{k_x+\mu k_y}{\varepsilon_{\vec{k}}}\\ \pm 1\end{pmatrix}, \tag{A17}$$

with energy

$$E = \pm\varepsilon_{\vec{k}} = \pm\sqrt{\cos^2\varphi|k_x+\nu k_y|^2 + \sin^2\varphi|k_x+\mu k_y|^2}. \tag{A18}$$

From (A17) we then obtain the Berry connection:

$$\begin{aligned}A_x^\pm &= \mathrm{Im}(\langle\Psi_\pm|\partial_{q_x}|\Psi_\pm\rangle)\\ &= -\frac{q_y}{2\varepsilon_{\vec{k}}^2}[\cos^2\varphi\mathrm{Im}(\nu) + \sin^2\varphi\mathrm{Im}(\mu)] \qquad \text{(A19a)}\\ A_y^\pm &= \frac{q_x}{2\varepsilon_{\vec{k}}^2}[\cos^2\varphi\mathrm{Im}(\nu) + \sin^2\varphi\mathrm{Im}(\mu)], \qquad \text{(A19b)}\end{aligned}$$

from which in turn we compute the Berry phase:

$$\gamma_\pm = \frac{1}{2\pi}\int_0^{2\pi} d\theta\frac{k^2}{\varepsilon_{\vec{k}}^2}[\cos^2\varphi\mathrm{Im}(\nu) + \sin^2\varphi\mathrm{Im}(\mu)]. \tag{A20}$$

Using the following formula:

$$\begin{aligned}&\frac{1}{2\pi}\int_0^{2\pi}\frac{d\theta}{\cos^2\theta + \rho^2\sin^2\theta + 2\rho\cos\phi\cos\theta\sin\theta}\\ &\quad = \frac{1}{\rho\sqrt{1-\cos^2\phi}},\end{aligned} \tag{A21}$$

we can recast the last expression (A20) into the form:

$$\gamma_\pm = \frac{\cos^2\varphi\mathrm{Im}(\nu) + \sin^2\varphi\mathrm{Im}(\mu)}{\sqrt{|\nu|^2\cos^2\varphi + |\mu|^2\sin^2\varphi - [\cos^2\varphi\mathrm{Re}(\nu) + \sin^2\varphi\mathrm{Re}(\mu)]^2}}. \tag{A22}$$

From (A22) we recover the Berry phase expressions (A14) and (A12) for the different models we considered. For the Berry phase (A22) to be topological, it must in particular be independent of φ, i.e., we must have $\partial_\varphi\gamma_\pm = 0\forall\varphi$. We find that this condition is fulfilled when and only when $\nu = \mu$, i.e., when the system is in duality class $\mathcal{D}_I$, according to (5). Here we have thus shown that for a three-band linear crossing with chiral symmetry to have a topological Berry phase, it must necessarily belong to duality class $\mathcal{D}_I$. Reciprocally we have shown in a previous section that any model in this class has a quantized topological Berry phase.

APPENDIX B: TRANSPORT PROPERTIES

1. Landauer conductivity

a. Matching conditions for $\vec{k}$-linear Hamiltonians

To solve the scattering problem through a tunnel junction, we want to compute the electronic wave functions in the different regions of the setup and ensure that the solutions obtained in neighbor regions satisfy the matching conditions at the interface. To this end, we want to derive matching conditions along the x direction for electronic wave packets described by a k-linear Hamiltonian $H = \vec{S}\cdot\vec{k}$. Let us consider an interface at $x = x_0$; the matching conditions at the interface derive from the continuity of the eigenvalue equation $\vec{S}\cdot\vec{k}\psi = (\varepsilon - V)\psi$, where $V(x < x_0) = V_1, V(x > x_0) = V_2$. Integrating the eigenvalue equation between $x_0 - \eta$ and $x_0 + \eta$ $(\eta > 0)$ gives:

$$S_x[\psi(x_0+\eta) - \psi(x_0-\eta)] = \int_{x_0-\eta}^{x_0+\eta} [\varepsilon - V(x)]\psi(x)dx, \tag{B1}$$

where we used $\vec{k} = -\mathrm{i}\frac{\partial}{\partial\vec{x}}$ in coordinate representation. Sending η to 0, the integral in the right-hand side of (B1) vanishes, yielding the following condition:

$$S_x \cdot \psi(x_0^-) = S_x \cdot \psi(x_0^+). \tag{B2}$$

Note that, in contrast with the usual case of the Schrödinger equation, for a k-linear Hamiltonian matching of the wave function does not imply continuity of the wave function's derivatives, but only of linear combinations of its components.

In the models we study, the presence of a chiral symmetry constrains the linearized low energy Hamiltonian to take the form (2) in the (A_1, A_2, B) basis. Hence, condition (B2) enforces the continuity of ψ_B at x_0, provided Λ_{11} or Λ_{21} is nonzero.

b. Derivation of the minimal conductivity in the $\mathcal{D}_I$ class

We now consider a given material in the $\mathcal{D}_I$ duality class: its low-energy excitations are described by Hamiltonian (A9). We now study the transmission of electronic current through a sample of dimensions $L \times W$ contacted between two electrodes, respectively at $x = 0$ and $x = L$. The chemical potential in the sample is set exactly at the band-touching point, whereas the electrodes are doped at a very large potential V_∞. Momentum in the transverse direction y is quantized in all three regions—the two electrodes and the sample. It is determined by the transverse boundary conditions: for instance, periodic boundary conditions give $q_y = \frac{2\pi n}{W}$.

The dimensionless dispersion relation in the electrodes writes: $V_\infty^2 = q_x^2 + q_y^2$. Since q_y is quantized and thus fixed, for a large enough potential V_∞ the normal incidence approximation $q_x/q_y \simeq 0$ becomes valid. Electronic wave functions [see Eq. (A10a)] in the left electrode then read:

$$\psi(x<0) = \frac{1}{\sqrt{2}}\begin{pmatrix}\alpha\\ \beta\\ 1\end{pmatrix}e^{\mathrm{i}\vec{q}\vec{r}} + \frac{r_n}{\sqrt{2}}\begin{pmatrix}-\alpha\\ -\beta\\ 1\end{pmatrix}e^{-\mathrm{i}\vec{q}\vec{r}}, \tag{B3}$$

and in the right electrode:

$$\psi(x>L) = \frac{t_n}{\sqrt{2}}\begin{pmatrix}\alpha\\ \beta\\ 1\end{pmatrix}e^{\mathrm{i}\vec{q}\vec{r}}. \tag{B4}$$

t_n and r_n are the transmission and reflexion amplitude of mode n.

In the sample, the Fermi level lies exactly at the nodal point $E = 0$. Evanescent zero-energy modes $\psi^T = (\psi_{A1}, \psi_{A2}, \psi_B)^T$ of Hamiltonian (A9) satisfy:

$$\psi_B(0<x<L) = Ce^{-\mathrm{i}\lambda q_y x + \mathrm{i}q_y y} \tag{B5a}$$

$$(\alpha^*\psi_{A1} + \beta^*\psi_{A2})(0<x<L) = C'e^{-\mathrm{i}\lambda^* q_y x + \mathrm{i}q_y y}. \tag{B5b}$$

Besides, matching conditions at the interfaces $x = 0$ and $x = L$, given by equation (B2), correspond to the continuity of ψ_B and $(\alpha^*\psi_{A1} + \beta^*\psi_{A2})$. Enforcing this continuity at $x = 0$ and $x = L$ and solving the system of equations yields for the transmission coefficient of mode n:

$$T_n = |t_n|^2 = \frac{1}{|\cosh(\mathrm{Im}(\lambda)q_n L)|^2}, \tag{B6}$$

where $q_y = q_n = \frac{2\pi n}{W}$. In the limit $W \gg L$, where we can neglect the impact of transverse boundary conditions, equation (B6) leads to the following expression for Landauer conductivity:

$$\sigma = \frac{L}{W}\frac{e^2}{h}\sum_n T_n = \frac{e^2}{\pi h}\frac{1}{\mathrm{Im}(\lambda)}. \tag{B7}$$

Note that the conductivity depends on the direction of the junction θ. The dependance can be carried out from (A9) taking into account the dependance of λ on θ. Assuming that $\theta = 0$ corresponds to a principal axis one finds that $\lambda(\theta) := \lambda_0$ is pure imaginary and the conductivity in the direction θ is given by

$$\sigma(\theta) = \frac{e^2}{\pi h}\left(\frac{1}{|\lambda_0|}\cos^2\theta + |\lambda_0|\sin^2\theta\right). \tag{B8}$$

The minimal conductivity takes its extrema values along the principal axes of the dispersion relation, $\sigma_1 = \frac{1}{|\lambda_0|}\frac{e^2}{\pi h}$ and $\sigma_2 = |\lambda_0|\frac{e^2}{\pi h}$. The determinant of the conductivity tensor reads straightforwardly from its expression in the principal axes basis: $\bar{\sigma} = \mathrm{diag}(\sigma_1, \sigma_2)$, which gives $\det\bar{\sigma} = (e^2/\pi h)^2$.

The H_3 model corresponds to $\lambda = -\mathrm{i}$, leading to $\sigma = \frac{e^2}{\pi h}$. Since the dispersion relation is isotropic in this case, the value of the minimal conductivity in the H_3 model is independent of the direction of the junction.

Note that reciprocally we have shown that any three-band chiral semimetal with finite minimal conductivity necessarily belongs to the $\mathcal{D}_I$ class. Indeed, a necessary condition for the existence of a minimal conductivity is given by (11) which, when it is fulfilled, implies in turn that the $\mathcal{D}_I$ criteria (5) is met.

c. Absence of minimal conductivity in the T_3 model

We study a strip of the T_3 material contacted between two electrodes, in a similar fashion as in the previous section. In the strip, the Fermi level is set at the band-touching point $E = 0$. Let us consider the propagation of an electronic wave

packet incident from the left electrode into the sample. In the strip, the zero-energy wave functions of (A6) must satisfy $\psi_B = 0$ (for $0 < \varphi < \pi/2$, $k_y \neq 0$). In the right electrode, the wave function is $\psi(x > L) = t_n \psi^+(\vec{q}) e^{i\vec{q}\vec{r}}$, where t_n gives the transmission coefficient of mode n: $T_n = |t_n|^2$ and ψ^+ is defined by Eq. (A5a). Thus, we have

$$\psi_B(0 < x < L) = 0 \tag{B9a}$$

$$\psi_B(x > L) = \frac{t_n}{\sqrt{2}} e^{i\vec{q}\vec{r}}. \tag{B9b}$$

Matching conditions (B2) enforce the continuity of ψ_B at the interface, leading to $t_n = 0$. This is true for all modes with nonzero transverse momentum k_y. Hence, the conductance $G = \frac{e^2}{h} \sum_n T_n$ can be zero or finite, independent of the system size, depending whether a mode with $k_y = 0$ is allowed or not by transverse boundary conditions. In any case, for the conductivity one finds:

$$\sigma = \frac{L}{W} \frac{e^2}{h} \sum_n T_n = 0 \tag{B10}$$

in the limit $W \gg L$.

2. Kubo conductivity of the T_3 model

We now compute the Kubo conductivity at the nodal point in the T_3 lattice. For simplicity we only show here the calculation in the case $t_1 = t_2$: the final result remains valid for any nonzero value of the hoppings. The low-energy Hamiltonian writes:

$$H(\vec{K} + \vec{q}) = \hbar v_F \begin{pmatrix} 0 & 0 & q_- \\ 0 & 0 & q_+ \\ q_+ & q_- & 0 \end{pmatrix}, \tag{B11}$$

where we denote $q_\pm = q_x \pm i q_y$, and with $v_F = 3at/2$, a the honeycomb lattice spacing and t the hopping strength.

We perform the computation using Kubo formula, which gives the linear response of the system at temperature $1/\beta$ to an ac electric field with frequency ω. Here we use the scheme that was introduced in Ref. [29] in the case of graphene: a phenomenological scattering rate $\eta > 0$ has to be introduced, which models a finite lifetime of the electronic excitations in the presence of electrodes and allows us to recover the Landauer conductivity within the Kubo formalism. The Kubo conductivity is computed in the limit of zero frequency and zero temperature, while keeping η finite. The final result for graphene is independent of η, a sign of the robustness of this material towards disorder.

The starting point is the Kubo formula:

$$\sigma_{\mu\nu}(\omega,\eta,\beta) = \frac{\hbar}{4\pi L^2} \int d\varepsilon \frac{f_\beta(\varepsilon + \hbar\omega) - f_\beta(\varepsilon)}{\hbar\omega} \times \mathrm{Tr}\left[G_\eta^{A-R}(\varepsilon) \hat{j}_\mu G_\eta^{A-R}(\varepsilon + \hbar\omega) \hat{j}_\nu \right], \tag{B12}$$

where $\eta > 0$ is the imaginary part of the self-energy, and f_β is the Fermi-Dirac distribution at temperature β^{-1}. The trace Tr runs over the basis of eigenstates of the T_3 Hamiltonian:

$$|\mathbf{q},\pm\rangle = \frac{1}{\sqrt{2}} \begin{pmatrix} \frac{1}{\sqrt{2}} e^{-i\theta} \\ \frac{1}{\sqrt{2}} e^{i\theta} \\ \pm 1 \end{pmatrix}, \quad \varepsilon_m = \pm\varepsilon(q) \equiv \pm\hbar v_F q$$

$$|\mathbf{q},0\rangle = \begin{pmatrix} -e^{-i\theta} \\ e^{i\theta} \\ 0 \end{pmatrix}, \quad \varepsilon_m = 0, \tag{B13}$$

with $q_\pm = q e^{\pm i\theta}$, $t_1 = t_2$. Performing the trace over (B13) in (B12) and taking the limits $\omega \to 0$, $\beta \to \infty$ while keeping $\eta > 0$, one finds:

$$\sigma_{\mathrm{Kubo}} = \frac{e^2}{\pi h} \left(1 + \int_0^\infty \frac{k^3 dk}{(\eta^2 + k^2)^2} \right) \to \infty. \tag{B14}$$

The integral in (B14) is divergent. The Kubo conductivity diverges for the T_3 model with a finite electronic lifetime; in particular we do not recover the Landauer conductivity (B10) $\sigma_{\mathrm{Landauer}} = 0$. We note that the result for Kubo conductivity result is consistent with the value obtained in the zero disorder limit in Ref. [30].

[1] J. Wang, H. Huang, W. Duan, and Z. Liu, J. Chem. Phys. **139**, 184701 (2013).

[2] W. Li, M. Guo, G. Zhang, and Y.-W. Zhang, Phys. Rev. B **89**, 205402 (2014).

[3] S. Katayama, A. Kobayashi, and Y. Suzumura, J. Phys. Soc. Jpn. **75**, 054705 (2006).

[4] M. O. Goerbig, J.-N. Fuchs, G. Montambaux, and F. Piéchon, Phys. Rev. B **78**, 045415 (2008).

[5] L. Lu, Z. Wang, D. Ye, L. Ran, L. Fu, J. D. Joannopoulos, and M. Soljacic, Science **349**, 622 (2015).

[6] S.-M. Huang, S.-Y. Xu, I. Belopolski, C.-C. Lee, G. Chang, B. Wang, N. Alidoust, G. Bian, M. Neupane, C. Zhang, S. Jin, A. Bansil, H. Lin, and M. Z. Hasan, Nature Commun. **6**, 7373 (2015).

[7] B. Q. Lv, H. M. Weng, B. B. Fu, X. P. Wang, H. Miao, J. Ma, P. Richard, X. C. Huang, L. X. Zhao, G. F. Chen, Z. Fang, X. Dai, T. Qian, and H. Ding, Phys. Rev. X **5**, 031013 (2015).

[8] S.-Y. Xu, I. Belopolski, N. Alidoust, M. Neupane, G. Bian, C. Zhang, R. Sankar, G. Chang, Z. Yuan, C.-C. Lee, S.-M. Huang, H. Zheng, J. Ma, D. S. Sanchez, B. Wang, A. Bansil, F. Chou, P. P. Shibayev, H. Lin, S. Jia, and M. Z. Hasan, Science **349**, 613 (2015).

[9] M. Orlita, D. M. Basko, M. S. Zholudev, F. Teppe, W. Knap, V. I. Gavrilenko, N. N. Mikhailov, S. A. Dvoretskii, P. Neugebauer, C. Faugeras, A.-L. Barra, G. Martinez, and M. Potemski, Nature Phys. **10**, 233 (2014).

[10] Z. Wang, Y. Sun, X.-Q. Chen, C. Franchini, G. Xu, H. Weng, X. Dai, and Z. Fang, Phys. Rev. B **85**, 195320 (2012).

[11] Z. K. Liu, B. Zhou, Y. Zhang, Z. J. Wang, H. M. Weng, D. Prabhakaran, S. K. Mo, Z. X. Shen, Z. Fang, X. Dai, Z. Hussain, and Y. L. Chen, Science **343**, 864 (2014).

[12] S.-Y. Xu, C. Liu, S. K. Kushwaha, R. Sankar, J. W. Krizan, I. Belopolski, M. Neupane, G. Bian, N. Alidoust, T.-R. Chang,

H.-T. Jeng, C.-Y. Huang, W.-F. Tsai, H. Lin, P. P. Shibayev, F.-C. Chou, R. J. Cava, and M. Z. Hasan, Science **347**, 294 (2015).
[13] Z. Wang, H. Weng, Q. Wu, X. Dai, and Z. Fang, Phys. Rev. B **88**, 125427 (2013).
[14] M. Neupane, S.-Y. Xu, R. Sankar, N. Alidoust, G. Bian, C. Liu, I. Belopolski, T.-R. Chang, H.-T. Jeng, H. Lin, A. Bansil, F. Chou, and M. Z. Hasan, Nature Commun. **5**, 3786 (2014).
[15] S. Borisenko, Q. Gibson, D. Evtushinsky, V. Zabolotnyy, B. Büchner, and R. J. Cava, Phys. Rev. Lett. **113**, 027603 (2014).
[16] S. M. Young, S. Zaheer, J. C. Y. Teo, C. L. Kane, E. J. Mele, and A. M. Rappe, Phys. Rev. Lett. **108**, 140405 (2012).
[17] J. A. Steinberg, S. M. Young, S. Zaheer, C. L. Kane, E. J. Mele, and A. M. Rappe, Phys. Rev. Lett. **112**, 036403 (2014).
[18] K. S. Novoselov, A. K. Geim, S. V. Morozov, D. Jiang, M. I. Katsnelson, I. V. Grigorieva, S. V. Dubonos, and A. A. Firsov, Nature (London) **438**, 197 (2005).
[19] M. I. Katsnelson, K. S. Novoselov, and A. K. Geim, Nature Phys. **2**, 620 (2006).
[20] J. Tworzydlo, B. Trauzettel, M. Titov, A. Rycerz, and C. W. J. Beenakker, Phys. Rev. Lett. **96**, 246802 (2006).
[21] Y. Zhang, Y.-W. Tan, H. L. Stormer, and P. Kim, Nature (London) **438**, 201 (2005).
[22] K. S. Novoselov, E. McCann, S. V. Morozov, V. I. Fal'ko, M. I. Katsnelson, U. Zeitler, D. Jiang, F. Schedin, and A. K. Geim, Nature Phys. **2**, 177 (2006).
[23] S. Murakami, New J. Phys. **9**, 356 (2007).
[24] H. A. Kramers and G. H. Wannier, Phys. Rev. **60**, 252 (1941).
[25] A. Raoux, M. Morigi, J.-N. Fuchs, F. Piéchon, and G. Montambaux, Phys. Rev. Lett. **112**, 026402 (2014).
[26] W. Hausler, Phys. Rev. B **91**, 041102(R) (2015).
[27] C. W. J. Beenakker, Rev. Mod. Phys. **69**, 731 (1997).
[28] C. W. Groth, M. Wimmer, A. R. Akhmerov, and X. Waintal, New J. Phys. **16**, 063065 (2014).
[29] S. Ryu, C. Mudry, A. Furusaki, and A. W. W. Ludwig, Phys. Rev. B **75**, 205344 (2007).
[30] M. Vigh, L. Oroszlány, S. Vajna, P. San-Jose, G. Dávid, J. Cserti, and B. Dóra, Phys. Rev. B **88**, 161413 (2013).
[31] B. Dora, J. Kailasvuori, and R. Moessner, Phys. Rev. B **84**, 195422 (2011).
[32] P. Baireuther, J. M. Edge, I. C. Fulga, C. W. J. Beenakker, and J. Tworzydło, Phys. Rev. B **89**, 035410 (2014).
[33] M. Trescher, B. Sbierski, P. W. Brouwer, and E. J. Bergholtz, Phys. Rev. B. **91**, 115135 (2015).